Progress In Electromagnetics Research M, Vol. 118, 93–104, 2023

OAM Beam Generation, Steering, and Limitations Using an Intelligent Reflecting Surface

Rafal Hazim, Nidal Qasem*, and Ahmad Alamayreh

Abstract—Orbital angular momentum (OAM) is a fundamental characteristic of electromagnetic waves and has gained significant attention in recent years because of its potential applications in various fields of radio and optics. Furthermore, OAM has been proposed as a means to increase the spectral efficiency of wireless communication systems. By encoding multiple independent data streams on different OAM modes of electromagnetic waves, OAM communication systems can increase the amount of information that can be transmitted over a single radio frequency channel. In this paper, we developed a new method for steering the OAM waves using an intelligent reflective surface (IRS) that is suitable for the far field. Specifically, we designed IRS coefficients to reflect and steer different multiplexed modes between different users based on OAM waves by controlling the IRS impedance, which can be varied depending on the beam steering direction. Moreover, we investigated the physical limitations of the IRS by noting the relations between the number of transmitted modes, IRS size, and impedance values in the IRS. Each impedance element in the IRS consists of real and imaginary values, and the negative values in the real part are used as an indication for reaching the physical limit. One suggestion to decrease the negative real values is by using windowing to decrease the beam waist. The proposed method may enable the extended coverage of OAM wireless communication.

1. INTRODUCTION

With the rapid development of emerging information networks, orbital angular momentum (OAM) can enable novel applications and allow for multiple access to wireless networks owing to its potential to improve spectral efficiency in wireless communications [1]. There are new technology domains in sixth-generation (6G) such as machine learning, artificial intelligence, blockchain, THz communication, OAM multiplexing, spatial modulation MIMO, and intelligent reflective surface (IRS). 6G must have a significantly higher data rate than fifth-generation (5G). While 20 Gbps was the targeted peak data rate for 5G, the target for 6G is a peak data rate of 1000 Gbps. To supply advanced multimedia services to a broad user base, the performance of the entire network must be improved, for instance by striving to achieve spectral efficiency that is twice as high as 5G. As a result, it is essential to develop new and innovative technologies that will allow future wireless network capacity to increase while maintaining a moderate and appropriate budget, complexity, and power consumption. One of these assumptions is that 6G technology will integrate OAM and IRS approaches [2].

For example, multiple independent data streams can be simultaneously transmitted and received using various OAM techniques. The OAM provides a new orthogonal resource by spatially distributing the helical phase front [3], and different OAM modes are mutually orthogonal, allowing for simultaneous and coaxial transmission for improved spectral efficiency [4]. Such waves are usually used in a variety of applications, including beam steering [5], cooperative OAM relaying systems [6], improving the spectrum efficiency of communications systems [7], and high-resolution imaging [8]. Various methods

Received 23 May 2023, Accepted 19 July 2023, Scheduled 4 August 2023
* Corresponding author: Nidal Qasem (ne.qasem@ammanu.edu.jo).
The authors are with the Communications and Computer Engineering Department, Al-Ahliyya Amman University, Amman, Jordan.

for generating OAM-carrying waves have been documented [9, 10], and their propagation properties have been studied [11], such as spiral phase plates antennas [12], uniform circular array (UCA) [13], metasurfaces [14], and circular traveling-wave antennas [15], which are commonly utilized in OAM multiplexing systems [16]. However, the UCA-based OAM communication system has several disadvantages, such as not being suitable for long-distance multiplexing and requiring a high degree of synchronization between the transmitting and receiving antennas. Furthermore, moving and reflection will destroy the orthogonality of OAM waves, thereby reducing the performance under non-line-of-sight (NLoS) conditions.

Notably, metasurfaces have an advanced ability to manipulate electromagnetic (EM) waves and have gradually become an enabling EM technology for next-generation wireless communications [17]. IRS is a metasurface that can program incident EM waves by adjusting the reflection coefficients and tuning the surface impedance, which is achieved through various mechanisms, including an applied electrical voltage [17], thermal excitation [18], optical pumping [18], and physical stretching [19]. The choice of IRS materials includes semiconductors [20] and graphene [21]. To date, a series of reports have focused on the remarkable features of the IRS to enhance the performance of wireless communication networks from various aspects [22, 23], such as spectral efficiency improvement [24, 25], coverage extension [26], and reliable transmission [27].

In [28], based on the alternate optimization strategy, an iterative method was suggested that optimizes the power distribution and phase changes of the IRS. In each iteration of the algorithm, the maximization-minimization based ℓ_1-ball projection approach yields the closed-form expression for the power allocation solution, and the weighted minimum mean square error-based fixed point iteration approach yields the locally optimal solution to IRS's reflecting phase shifts. In [29], IRS was used to assist in the transmission of OAM-based multiplexed signals by combining the IRS with OAM-based rate-splitting multiple access schemes. In [30], the researchers suggested a method for IRS-assisted OAM multiplexing that eliminated the inter-mode interference (IMI) from all OAM modes. In addition, they have proposed an ℓ_2-ball projection method to optimize the transmit power allocation for OAM modes to increase the system capacity of IRS-assisted OAM communication systems. The IMI cancellation method and ℓ_2-ball projection method can increase the maximum system capacity compared with the ℓ_1-ball projection method when the IRS is located closer to the center between the transmitter UCA and receiver UCA.

In [31], an IRS-assisted multi-user OAM communication system was proposed to improve capacity and overcome the NLoS condition. The conventional OAM system generally performed well in the short-range and line-of-sight (LoS) scenarios. However, the capacity of wireless OAM-based multiple inputs and multiple outputs can be improved by deploying an IRS for a large number of reconfigurable passive elements to control the wireless propagation environment [32]. In [33], the authors proposed a multi-OAM-mode vortex wave multiplexing and demultiplexing scheme based on a shared-aperture reflective metasurface. The specifically designed reflective metasurface can realize the corresponding OAM-mode modulations and demodulations of different incident carrier waves in the corresponding data channels. By modulating multiple data channels on multiple OAM modes, multiplication of the communication capacity can be achieved.

In [34], three reflective metasurfaces with single and dual-directed OAM beams were proposed to tackle the poor network coverage of terahertz (THz) waves in the absence of LoS communications. The integration between the OAM and THz reflective metasurface technologies is a low-cost and low-profile solution for improving spectral efficiency. The OAM multiplexing and demultiplexing based on a single metasurface may provide a route for high-capacity and compact free-space communication systems. In [35], OAM multiplexing and demultiplexing at the E-band frequency using a single metasurface structure were proposed and experimentally demonstrated. For OAM multiplexing, the metasurface was used as a transceiver to generate two orthogonal coaxial OAM beams for Gaussian incident beams with different incidence angles. For OAM demultiplexing, the same metasurface flipped 180° was used as a receiver to form a Gaussian beam in different off-axis directions depending on the topological charge of the coaxially incident OAM beam.

In this paper, we developed a new method for steering the OAM waves using an IRS for far-field applications. We designed the IRS reflection coefficients to reflect and steer different multiplexed modes between the IRS and users based on OAM waves by controlling the IRS impedance, which can be

varied depending on the beam steering direction. We used the reflection coefficients to calculate the impedance value for each element in the IRS instead of the transmission coefficients in order to get rid of the sheet thickness calculation because it is more complicated. Each element in the IRS consists of real and imaginary values, and the negative values in the real part will be neglected. In addition, we decreased the negative values that appeared in the real values by changing the Gaussian waist value, and it can also be done by increasing the sheet size. In other work, real values are neglected, and imaginary values are used to design the sheet [36]. The proposed method may have a significant advantage in expanding the coverage of OAM wireless communication while considering the physical size limitation for the IRS and controlling its reflection coefficients. Ultimately, this was achieved by employing the back-propagation technique.

This paper is structured as follows. Section 2 includes a general overview of the system model and derivation of the field expression. Section 3 provides the simulation results based on the derived formulas using MATLAB. Then, it compares the current work with previous works. Finally, the conclusions are summarized in Section 4.

2. SYSTEM MODEL

In this study, we apply a single IRS to simultaneously generate several OAM wave vorticities in various directions and with various modes, as shown in Fig. 1(a). The suggested approach may help to increase OAM wireless communication coverage.

A mathematical formula, based on Fig. 1(b), is provided for designing the generated wave by creating an initial beam from a Bessel beam of OAM mode $m = 1$. A Bessel function of the first kind and the order J_m determines the beam's amplitude in the plane of transverse propagation.

$$E_{Desired} = J_m(\sqrt{(x+x_o)^2+(y+y_o)^2})((x+x_o)+(y+y_o)sign(m)i)^{|m|}e^{-\frac{(x+x_o)^2+(y+y_o)^2}{W_o^2}} \tag{1}$$

where W_o is the Gaussian beam waist, (x_o, y_o) used for shifting the target of the beam, *sign* a signum function, and (x, y, z) the coordinate system. The far field can be determined using the Fresnel diffraction formula [37]:

$$E_z(x,y,z) = -\frac{i}{\lambda z}e^{ikz}e^{\frac{ik}{2z}(x^2+y^2)}\iint E_o\left(x',y'\right)e^{\frac{ik}{2z}\left(x'^2+y'^2\right)}e^{\frac{-i2\pi}{\lambda z}(x'x+y'y)}dx'dy' \tag{2}$$

where E_o is the desired field, $z = 10\lambda$ the location of the observation window, $\lambda = 0.015\,\mathrm{m}$ the wavelength, and $k = 2\pi/\lambda$ the wavenumber. Let $f_x = \frac{x}{\lambda z}$, and $f_y = \frac{y}{\lambda z}$ then:

$$E_z(x,y,z) = -\frac{i}{\lambda z}e^{ikz}e^{\frac{ik}{2z}(x^2+y^2)}\iint E_o\left(x',y'\right)e^{\frac{ik}{2z}\left(x'^2+y'^2\right)}e^{-i2\pi f_x x'}e^{-i2\pi f_y y'}dx'dy' \tag{3}$$

We can also use the Fourier transform formula instead of the integral form in Eq. (3).

$$\iint E_z\left(x',y'\right)e^{\frac{ik}{2z}\left(x'^2+y'^2\right)}e^{-i2\pi f_x x'}e^{-i2\pi f_y y'}dx'dy' = F\left\{E_o(x',y')\,e^{\frac{ik}{2z}\left(x'^2+y'^2\right)}\right\}$$

$$E_z(x,y,z) = -\frac{i}{\lambda z}e^{ikz}e^{\frac{ik}{2z}\left(x^2+y^2\right)}F\left\{E_o(x',y')\,e^{\frac{ik}{2z}\left(x'^2+y'^2\right)}\right\} \tag{4}$$

To find the near field using the backward Fresnel diffraction formula, we can obtain $E_o(x', y')$ at the source by backward diffraction and using the inverse Fourier transform formula

$$E_o\left(x',y'\right) = (-i\lambda z)e^{ikz}e^{\frac{ik}{2z}\left(x'^2+y'^2\right)}F^{-1}\left\{E_z(x,y,z)\,e^{\frac{ik}{2z}\left(x^2+y^2\right)}\right\} \tag{5}$$

Additionally, we can use the integral form instead of the inverse Fourier transform formula used in Eq. (5).

$$F^{-1}\left\{E_z(x,y,z)\,e^{\frac{ik}{2z}\left(x^2+y^2\right)}\right\} = \iint E_z(x,y,z)\,e^{\frac{ik}{2z}\left(x^2+y^2\right)}e^{i2\pi f_{x'}x'}e^{i2\pi f_{y'}y'}dxdy \tag{6}$$

let $f_{x'} = \frac{x'}{\lambda z}$, and $f_{y'} = \frac{y'}{\lambda z}$, and we could finally obtain:

$$E_o\left(x',y'\right) = (-i\lambda z)\,e^{ikz}e^{\frac{ik}{2z}\left(x'^2+y'^2\right)}\iint E_z(x,y,z)\,e^{\frac{ik}{2z}\left(x^2+y^2\right)}e^{\frac{2\pi}{\lambda z}\left(x'^2+y'^2\right)}dxdy \tag{7}$$

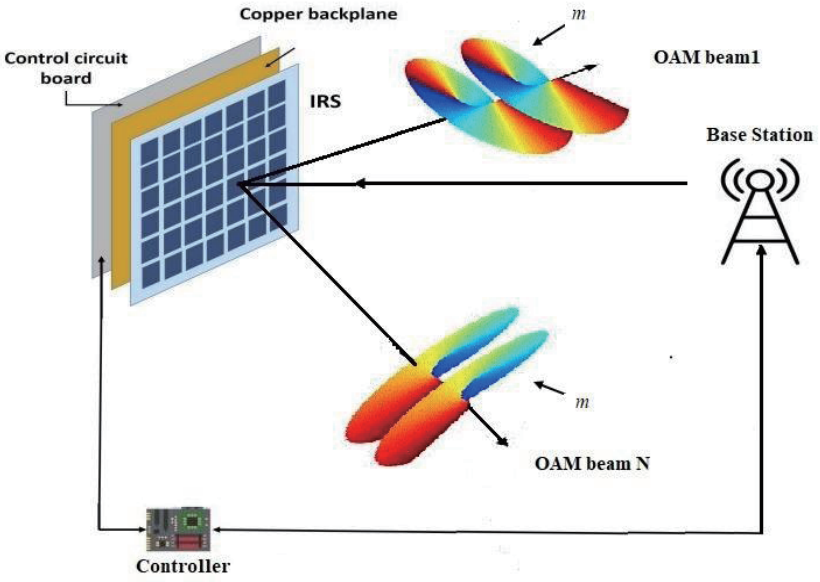

(a)

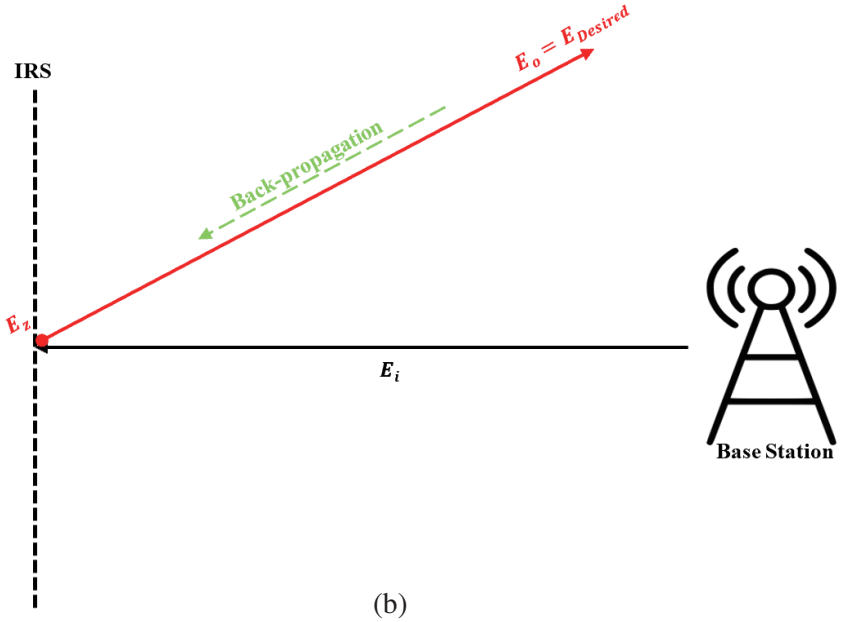

(b)

Figure 1. The typical implementation of the IRS design based on OAM waves. (a) Block diagram. (b) Schematic of the communication system.

Then, we calculate the reflection coefficient using Eq. (8). The objective of the impedance calculation is to control the elements of the IRS sheet and to determine which elements reflect the OAM wave because the element is either considered on or off according to the impedance value [38].

$$\Gamma = \frac{E_r}{E_i} \tag{8}$$

where Γ is the reflection coefficient, E_i the incidence wave for the plate, and E_r the reflected wave for the plate, which we find from the near field (E_z). Furthermore, Γ is determined by the impedance and can be represented by the following equation:

$$\Gamma = \frac{(Z_s - Z_0)}{(Z_s + Z_0)} \tag{9}$$

where Z_s is the impedance of the plate, and $Z_0 = 377\Omega$ is the free-space impedance. We use Eq. (9) to find the Z_s value, considering that the Γ and Z_0 values are known. Through Eq. (9), the impedance value of each element in the IRS can be calculated. The impedance value of each element in the IRS consists of a real part and an imaginary part. In the real part, which consists of positive or negative values, we ignore the negative values by setting them to zero and retain the value of the imaginary part.

3. RESULTS AND DISCUSSION

To appreciate the capability of the steering method and evaluate the credibility of the derived model, the results obtained from numerical simulations using MATLAB are provided. First, we determine the essential factors for OAM waves generation and steering. Then, we examine the method for the near field based on the generated OAM waves using the IRS. Second, we evaluate the multi-beam reflections of the OAM waves and steer them using the IRS for the far field considering the physical size limitation for the IRS and controlling its elements.

In the first case, we use one beam, while the size of the IRS sheet is fixed ($10\lambda \times 10\lambda$), and the value of the Gaussian beam waist W_o changes. The positive values of the impedance decrease as the values of the W_o increase, as shown in Table 1. As a result, the distortion increases with increasing W_o because the greater the W_o is, the interference with the next beam increases, or in other words if the size of the beam is reduced, the size of the IRS sheet can be larger.

Table 1. Generating one OAM beam at mode 1 with different Gaussian waists (W_o) using an IRS sheet with the size of ($10\lambda \times 10\lambda$).

Case No.	W_o/λ	Positive values	Negative values
1	0.5	100%	0%
2	0.75	70.4166%	29.5834%
3	1	59.2683%	40.7317%
4	1.25	54.1992%	45.8008%
5	1.5	57.2288%	42.7712%
6	1.75	60.3475%	39.6525%
7	2	62.1594%	37.8406%
8	2.25	59.3376%	40.6624%
9	2.5	49.3577%	50.6423%
10	2.75	46.9518%	53.0482%
11	3	38.7936%	61.2064%

Figure 2 shows the numerical simulation results of radio OAM vortex waves with different Gaussian waists (W_o) for one beam with a fixed size of the IRS sheet ($10\lambda \times 10\lambda$). Notably, the transmitted wave is not affected after its reflection from the IRS when the value of $W_o = 0.5\lambda$. Although there are minor distortions in the phase compared with the transmitter, the amplitude is unchanged. Fig. 3 shows that, for $W_o = 3\lambda$, the distortion increases in phase and amplitude for the near field and far field because the positive impedance values decrease, and the negative impedance values increase for the elements of the IRS, as shown in Table 1.

In the second case, we use four OAM beams while the size of the sheet is fixed ($10\lambda \times 10\lambda$) and the value of $W_o = 0.5\lambda$. The positive values of the impedance decrease as the number of beams increases, as summarized in Table 2.

Figures 4, 5, and 6 show the numerical simulation results of multi-OAM beams for a fixed IRS sheet size of ($10\lambda \times 10\lambda$) and $W_o = 0.5\lambda$. When one OAM beam is utilized, the impedance values are all positive. However, when two OAM beams are utilized at once, the positive impedance values drop, and the negative values become apparent. Additionally, while three OAM beams are utilized simultaneously, the positive impedance values decrease, and the negative values increase. When the number of beams

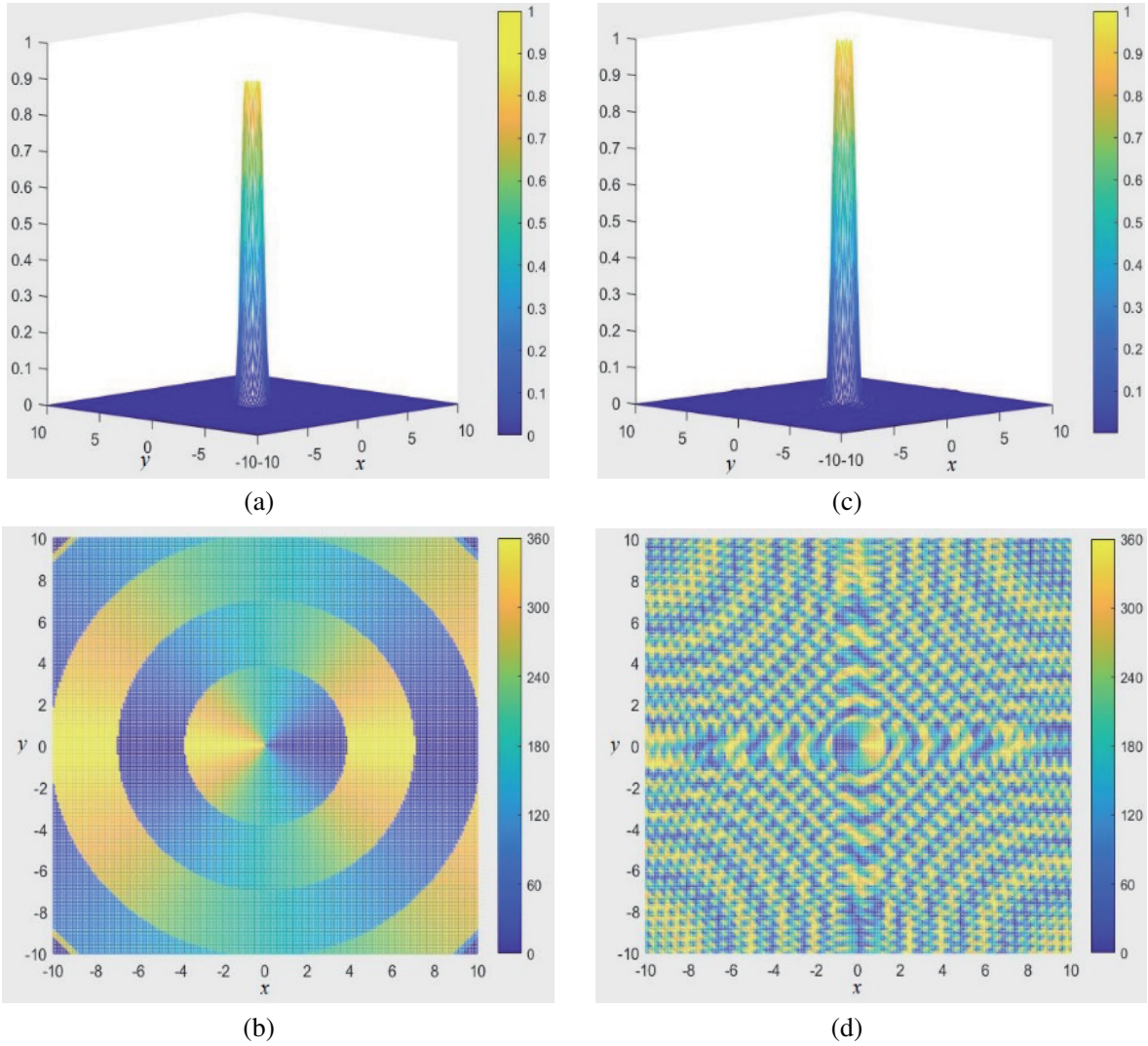

Figure 2. The electric field for generating one OAM beam when the IRS sheet size is $(10\lambda \times 10\lambda)$ and $W_o = 0.5\lambda$. (a) The desired one beam (amplitude). (b) The desired one beam (phase). (c) The far field was obtained for one beam (amplitude). (d) The far field was obtained for one beam (phase).

Table 2. Different OAM beams for the IRS sheet size of $(10\lambda \times 10\lambda)$ and $W_o = 0.5\lambda$.

Case No.	No. of beams	Positive values	Negative values
1	One	100	0
2	Two	91.5274	8.4726
3	Three	78.1095	21.8905
4	Four	66.2187	33.7813

is extended to four, the positive impedance values decrease further, and the negative values increase. We conclude that distortion rises when the number of OAM beams increases, as indicated in Table 2.

Next, our proposed system is compared to the other generating OAM techniques reported in [1, 33, 34] with respect to generating techniques, number of modes, operating frequency, and steering capability, as summarized in Table 3. In [1], the authors used the UCA factor formulated in cylindrical

coordinates to express the electric field of antennas arrayed for generating OAM. They programmed the OAM-UCA factor in cylindrical coordinates and used it to optimize the radiation performance while generating OAM modes. In [33], this study proposed a multiple OAM-mode vortex-beam multiplexing and demultiplexing scheme based on the shared aperture reflective metasurface by dual-channel reflective metasurface for two OAM-mode multiplexing and four-channel reflective metasurface for four OAM-mode multiplexing. In [34], this study proposed three reflective metasurfaces with single and dual-directed OAM beams to tackle the poor network coverage of THz waves in the absence of LoS communications. Through integration between the OAM and THz reflective metasurface technologies can improve spectral efficiency through a low-cost and low-profile solution. By comparing our work to earlier studies, we were able to address the difficulties of generating OAM waves by combining them with the IRS technique. We solved the problem of guiding the wave to a dead zone with no network connectivity using IRS by managing the IRS elements. We overcame OAM challenges like diverging and coverage by steering the OAM waves in a far field. Furthermore, we employed the IRS to steer more than one OAM beam to specified points, thereby enhancing capacity while also increasing network coverage.

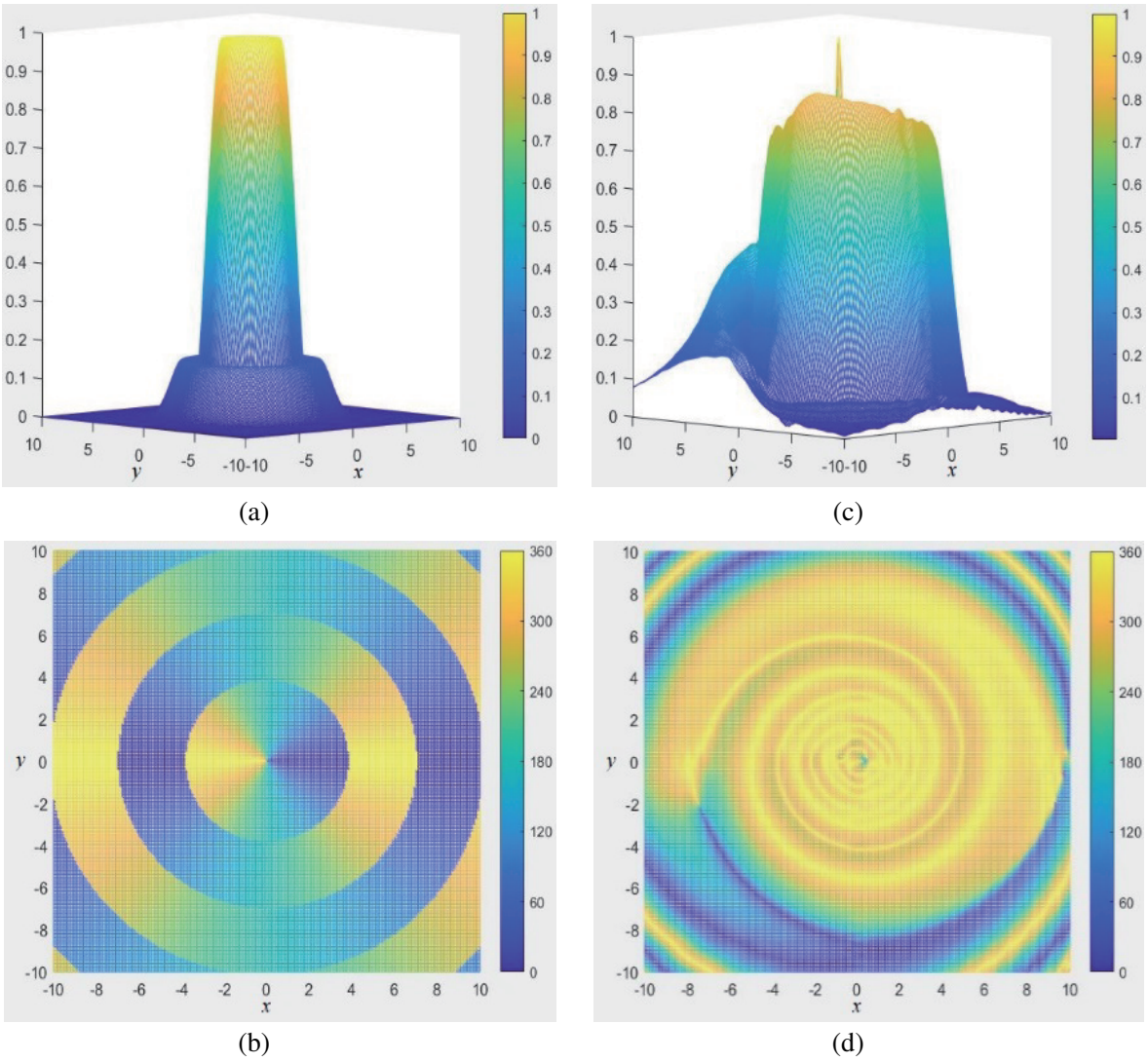

Figure 3. The electric field for generating one OAM beam when the IRS sheet size is $(10\lambda \times 10\lambda)$ and $W_o = 3\lambda$. (a) The desired one beam (amplitude). (b) The desired one beam (phase). (c) The far field was obtained for one beam (amplitude). (d) The far field was obtained for one beam (phase).

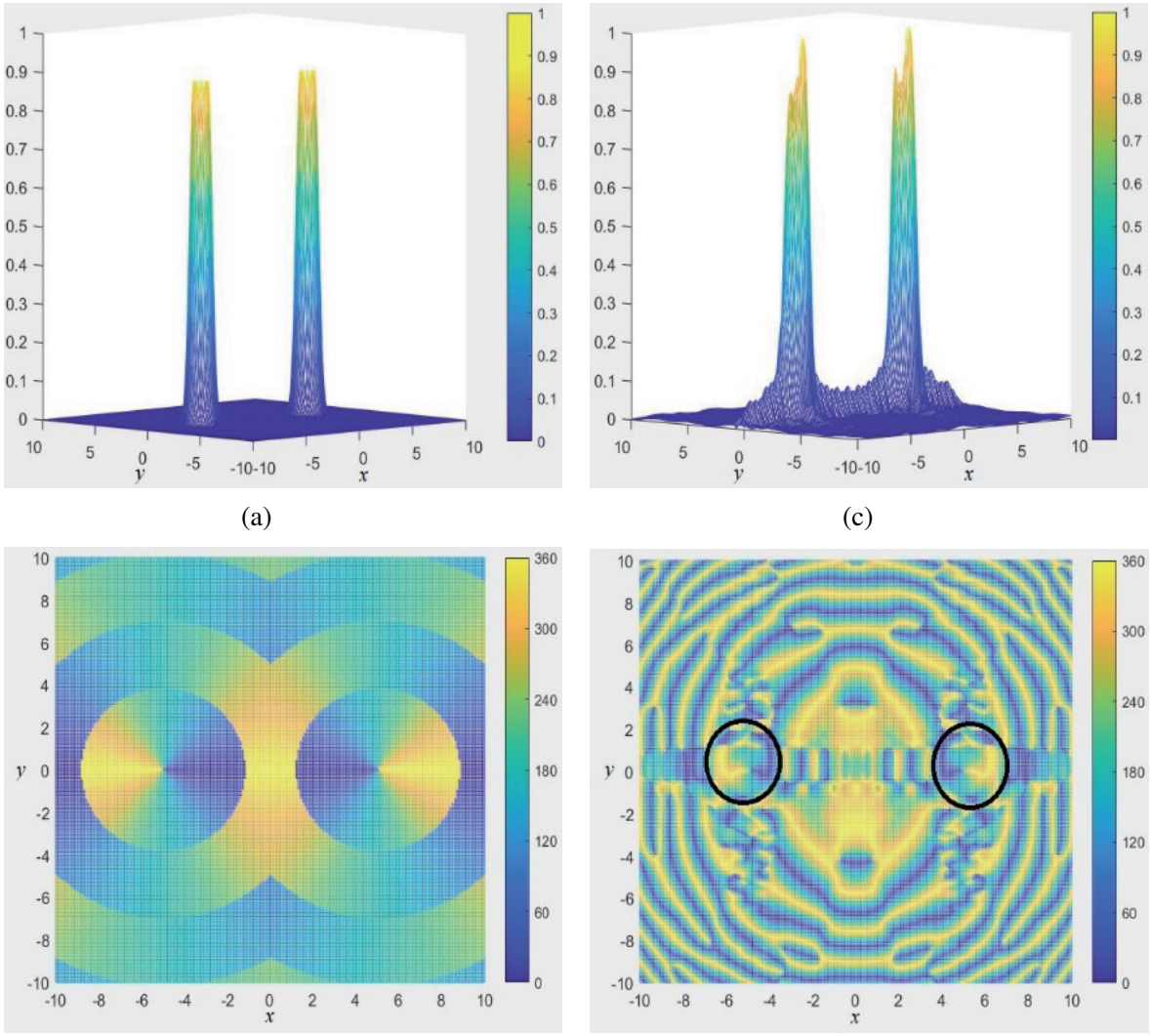

Figure 4. The electric field for generating two OAM beams when the IRS sheet size is $(10\lambda \times 10\lambda)$ and $W_o = 0.5\lambda$. (a) The desired two beams (amplitude). (b) The desired two beams (phase). (c) The far field was obtained for two beams (amplitude). (d) The far field was obtained for two beams (phase).

Table 3. Comparison of the suggested system performance with previously developed generating OAM techniques.

References	Generating Technique	No. of Modes	Operating Frequency	Steering Capability
[1]	UCA	Single-mode	73 GHz	Not applicable
[33]	Reflective metasurface	Dual-mode	10 GHz	Not applicable
[34]	Reflective metasurface	Multi-mode	90–110 GHz	Not applicable
This work	IRS	Multi-mode	Wide range	Dynamic

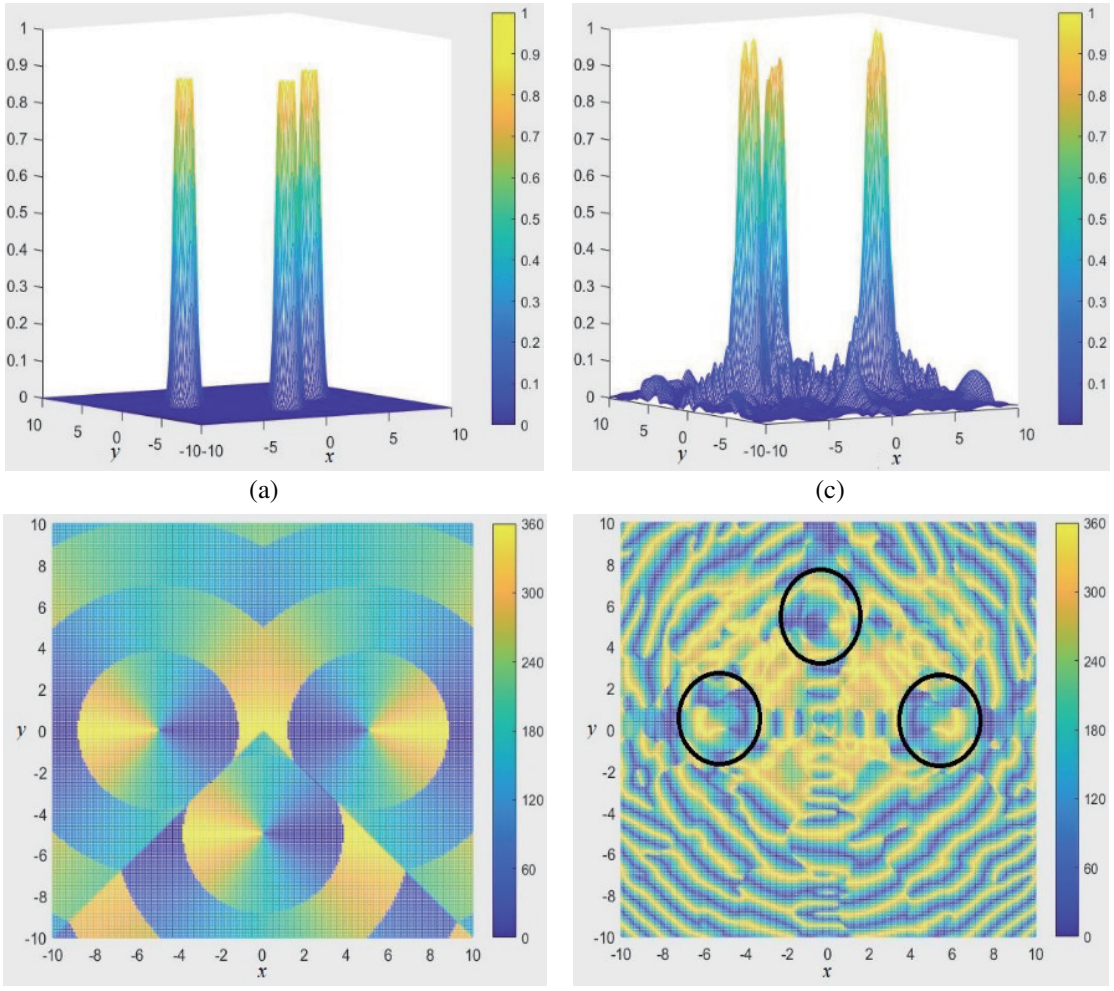

Figure 5. The electric field for generating three OAM beams when the IRS sheet size is $(10\lambda \times 10\lambda)$ and $W_o = 0.5\lambda$. (a) The desired three beams (amplitude). (b) The desired three beams (phase). (c) The far field was obtained for three beams (amplitude). (d) The far field was obtained for three beams (phase).

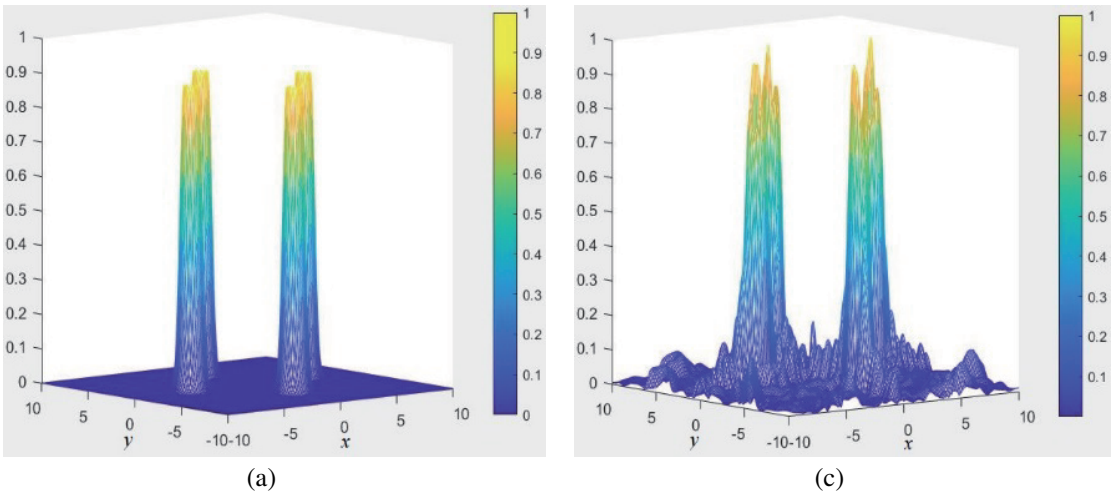

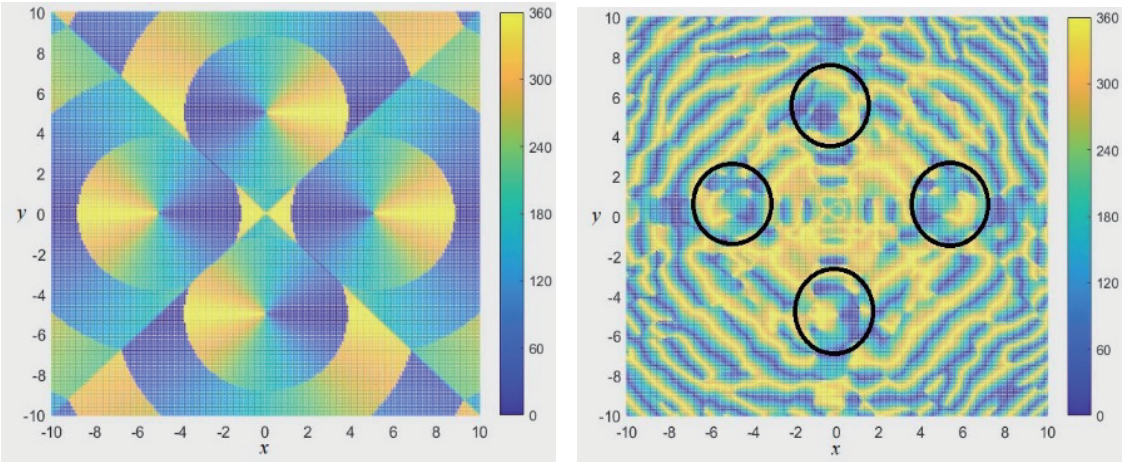

(b) (d)

Figure 6. The electric field for generating four OAM beams when the IRS sheet size is $(10\lambda \times 10\lambda)$ and$W_o = 0.5\lambda$. (a) The desired four beams (amplitude). (b) The desired four beams (phase). (c) The far field was obtained for four beams (amplitude). (d) The far field was obtained for four beams (phase).

4. CONCLUSIONS

In this paper, we developed a new method for steering the OAM wave using an IRS that is suitable for far-field applications. We designed the IRS reflection coefficients to reflect and steer different multiplexed modes between the IRS and users based on OAM waves by considering the physical size limitation of the IRS and controlling its elements, which vary depending on the beam steering direction for the far field. We used the reflection coefficients to calculate the impedance value for each element in the IRS instead of the transmission coefficients equation in order to get rid of the sheet thickness calculation. Each element in the IRS consists of real and imaginary values, and the negative values in the real part have been neglected. In addition, we decreased the negative values that appeared in the real values by changing the Gaussian waist value, and it can also be done by increasing the sheet size. Assuming that the size of the IRS sheet is fixed, and W_o is variable, we achieved this by employing the back-propagation technique. In the first case, we examined one OAM beam reflected from IRS and determined the size of the sheet $(10\lambda \times 10\lambda)$ and the waist value $W_o = 0.5\lambda$. In the second case, we examined four OAM beams reflected from the IRS for the fixed IRS sheet size $(10\lambda \times 10\lambda)$ and $W_o = 0.5\lambda$ because it was considered the optimal value. In both cases, the positive values of the impedance decreased, and distortion in the OAM wave increased with the increase in the number of beams and the value of W_o.

REFERENCES

1. Fang, L. and R. M. Henderson, "Orbital angular momentum uniform circular antenna array design and optimization-based array factor," *2019 IEEE Texas Symposium on Wireless and Microwave Circuits and Systems (WMCS)*, 1–4, Waco, TX, USA, 2019.
2. Akhtar, M. W., S. A. Hassan, R. Ghaffar, H. Jung, S. Garg, and M. S. Hossain, "The shift to 6G communications: Vision and requirements," *Human-centric Computing and Information Sciences*, Vol. 10, No. 1, 1–27, 2020.
3. Alamayreh, A. and N. Qasem, "Vortex beam generation in microwave band," *Progress In Electromagnetics Research C*, Vol. 107, 49–63, 2021.
4. Allen, L., M. W. Beijersbergen, R. J. Spreeuw, and J. P. Woerdman, "Orbital angular momentum of light and the transformation of Laguerre-Gaussian laser modes," *Physical Review A*, Vol. 45, No. 11, 8185–8189, 1992.

5. Qasem, N., A. Alamayreh, and J. Rahhal, "Beam steering using OAM waves generated by a concentric circular loop antenna array," *Wireless Networks*, Vol. 27, No. 4, 2431–2440, 2021.
6. Alkhawatrah, M., A. Alamayreh, and N. Qasem, "Cooperative relay networks based on the OAM technique for 5G applications," *Computer Systems Science & Engineering*, Vol. 44, No. 3, 1911–1919, 2023.
7. Alamayreh, A., N. Qasem, and J. S. Rahhal, "General configuration MIMO system with arbitrary OAM," *Electromagnetics*, Vol. 40, No. 5, 343–353, 2020.
8. Liu, K., Y. Cheng, Y. Gao, X. Li, Y. Qin, and H. Wang, "Super-resolution radar imaging based on experimental OAM beams," *Applied Physics Letters*, Vol. 110, No. 16, 164102, 2017.
9. Yang, Y., K. Guo, F. Shen, Y. Gong, and Z. Guo, "Generating multiple OAM based on a nested dual-arm spiral antenna," *IEEE Access*, Vol. 7, 138541–138547, 2019.
10. Noor, S. K., M. N. M. Yasin, A. M. Ismail, M. N. Osman, P. J. Soh, N. Ramli, and A. H. Rambe, "A review of orbital angular momentum vortex waves for the next generation wireless communications," *IEEE Access*, Vol. 10, 89465–89484, 2022.
11. Wang, L., W. Park, C. Yang, H.-D. Bruns, D. G. Kam, and C. Schuster, "Wireless communication of radio waves carrying orbital angular momentum (OAM) above an infinite ground plane," *IEEE Transactions on Electromagnetic Compatibility*, Vol. 62, No. 5, 2257–2264, 2020.
12. Yao, H., H. Kumar, T. Ei, S. Sharma, R. Henderson, S. Ashrafi, D. MacFarlane, Z. Zhao, Y. Yan, and A. Willner, "Experimental demonstration of a dual-channel E-band communication link using commercial impulse radios with orbital angular momentum multiplexing," *2017 IEEE Radio and Wireless Symposium (RWS)*, 51–54, Phoenix, AZ, USA, 2017.
13. Fang, L., H. Yao, and R. M. Henderson, "OAM antenna arrays at E-band," *2017 IEEE MTT-S International Microwave Symposium (IMS)*, 658–661, Honololu, HI, USA, 2017.
14. Yu, N. and F. Capasso, "Flat optics with designer metasurfaces," *Nature Materials*, Vol. 13, No. 2, 139–150, 2014.
15. Wang, R., M. Wang, Y. Zhang, D. Liao, and L. Jing, "Generation of orbital angular momentum multiplexing millimeter waves based on a circular traveling wave antenna," *Optics Express*, Vol. 31, No. 3, 5131–5139, 2023.
16. Hui, X., S. Zheng, Y. Chen, Y. Hu, X. Jin, H. Chi, and X. Zhang, "Multiplexed millimeter wave communication with dual orbital angular momentum (OAM) mode antennas," *Scientific Reports*, Vol. 5, No. 1, 10148, 2015.
17. Sideeq, M. M. M. and N. Qasem, "Smart wall based on active frequency selective wallpaper," *ZANCO Journal of Pure and Applied Sciences*, Vol. 28, No. 2, 1–6, 2016.
18. Sharma, T., A. Chehri, and P. Fortier, "Reconfigurable intelligent surfaces for 5G and beyond wireless communications: A comprehensive survey," *Energies*, Vol. 14, No. 24, 8219, 2021.
19. Liu, Y., X. Liu, X. Mu, T. Hou, J. Xu, M. Di Renzo, and N. Al-Dhahir, "Reconfigurable intelligent surfaces: principles and opportunities," *IEEE Communications Surveys & Tutorials*, Vol. 23, No. 3, 1546–1577, 2021.
20. Abeywickrama, S., R. Zhang, Q. Wu, and C. Yuen, "Intelligent reflecting surface: Practical phase shift model and beamforming optimization," *IEEE Transactions on Communications*, Vol. 68, No. 9, 5849–5863, 2020.
21. Marhoon, H. M., N. Qasem, N. B. Mohamad, and A. R. Ibrahim, "Design and simulation of a compact metal-graphene frequency reconfigurable microstrip patch antenna with FSS superstrate for 5G applications," *International Journal on Engineering Applications (IREA)*, Vol. 10, No. 3, 193–201, 2022.
22. Wu, Q., S. Zhang, B. Zheng, C. You, and R. Zhang, "Intelligent reflecting surface-aided wireless communications: A tutorial," *IEEE Transactions on Communications*, Vol. 69, No. 5, 3313–3351, 2021.
23. Gong, S., X. Lu, D. T. Hoang, D. Niyato, L. Shu, D. I. Kim, and Y. C. Liang, "Toward smart wireless communications via intelligent reflecting surfaces: A contemporary survey," *IEEE Communications Surveys & Tutorials*, Vol. 22, No. 4, 2283–2314, 2020.

24. Yang, Z., Y. Hu, Z. Zhang, W. Xu, C. Zhong, and K.-K. Wong, "Reconfigurable intelligent surface based orbital angular momentum: Architecture, opportunities, and challenges," *IEEE Wireless Communications*, Vol. 28, No. 6, 132–137, 2021.
25. Wu, Q. and R. Zhang, "Intelligent reflecting surface enhanced wireless network via joint active and passive beamforming," *IEEE Transactions on Wireless Communications*, Vol. 18, No. 11, 5394–5409, Nov. 2019.
26. Han, Y., W. Tang, S. Jin, C.-K.Wen, and X. Ma, "Large intelligent surface assisted wireless communication exploiting statistical CSI," *IEEE Transactions on Vehicular Technology*, Vol. 68, No. 8, 8238–8242, 2019.
27. Cui, M., G. Zhang, and R. Zhang, "Secure wireless communication via intelligent reflecting surface," *IEEE Wireless Communications Letters*, Vol. 8, No. 5, 1410–1414, 2019.
28. Li, Y., M. Jiang, G. Zhang, and M. Cui, "Achievable rate maximization for intelligent reflecting surface-assisted orbital angular momentum-based communication systems," *IEEE Transactions on Vehicular Technology*, Vol. 70, No. 7, 7277–7282, 2021.
29. Qayyum, A. and S. Y. Shin, "Capacity analysis Of IRS Assisted RSMA-OAM for next generation of wireless communication," *Proceedings of the Korean Telecommunications Society Conference*, 79–80, Seoul, South Korea, 2023.
30. Ono, K., K. Yoshii, M. Saito, Z. Pan, J. Liu, and S. Shimamoto, "Performance analysis of intelligent reflecting surface-assisted orbital angular momentum-based communication systems," *2022 24th International Conference on Advanced Communication Technology (ICACT)*, 7–12, PyeongChang, Republic of Korea, 2022.
31. Lee, H. Y. and S. Y. Shin, "Reconfigurable intelligent surface assisted multi-user orbital angular momentum communications," *2022 13th International Conference on Information and Communication Technology Convergence (ICTC)*, 1597–600, Jeju Island, Republic of Korea, Oct. 2022.
32. Wang, Y., N. Cyprien, T. Hu, and X. Liao, "IRS aided OAM-MIMO communication," *2021 International Symposium on Antennas and Propagation (ISAP)*, 1–2, Taipei, Taiwan, 2021.
33. Feng, Q., X. Kong, M. Shan, Y. Lin, L. Li, and T. J. Cui, "Multi-orbital-angular-momentum-mode vortex wave multiplexing and demultiplexing with shared-aperture reflective metasurfaces," *Physical Review Applied*, Vol. 17, No. 3, 2022.
34. Ali, A., M. Khalily, D. Serghiou, and R. Tafazolli, "Reflective metasurface with steered OAM beams for THz communications," *IEEE Access*, Vol. 11, 12394–12401, 2023.
35. Chung, H., D. Kim, E. Choi, and J. Lee, "E-band metasurface-based orbital angular momentum multiplexing and demultiplexing," *Laser & Photonics Reviews*, Vol. 16, No. 6, 2100456, 2022.
36. Grbic, A. and R. Merlin, "Near-field focusing plates and their design," *IEEE Transactions on Antennas and Propagation*, Vol. 56, No. 10, 3159–3165, 2008.
37. Peatross, J. and M. Ware, "Physics of light and optics," *Brigham Young University*, 2015.
38. Cai, W., R. Liu, Y. Liu, M. Li, and Q. Liu, "Intelligent reflecting surface assisted multi-cell multi-band wireless networks," *2021 IEEE Wireless Communications and Networking Conference (WCNC)*, 1–6, Nanjing, China, 2021.